Available online at www.sciencedirect.com
ScienceDirect
Journal of Sound and Vibration 297 (2006) 536–550
JOURNAL OF SOUND AND VIBRATION
www.elsevier.com/locate/jsvi

Application of continuous wavelet transform in vibration based damage detection method for beams and plates

M. Rucka*, K. Wilde

Faculty of Civil and Environmental Engineering, Gdańsk University of Technology, Gdańsk, Poland

Received 4 July 2005; received in revised form 13 March 2006; accepted 4 April 2006
Available online 21 June 2006

Abstract

In this paper a method for estimating the damage location in beam and plate structures is presented. A Plexiglas cantilever beam and a steel plate with four fixed boundary conditions are tested experimentally. The estimated mode shapes of the beam are analysed by the one-dimensional continuous wavelet transform. The formulation of the two-dimensional continuous wavelet transform for plate damage detection is presented. The location of the damage is indicated by a peak in the spatial variation of the transformed response. Applications of Gaussian wavelet for one-dimensional problems and reverse biorthogonal wavelet for two-dimensional structures are presented. The proposed wavelet analysis can effectively identify the defect position without knowledge of neither the structure characteristics nor its mathematical model.

1. Introduction

The application of wavelet transforms to a wide variety of problems is so plentiful that they have emerged as the most promising techniques in the past decade. Wavelets help to analyse variations of values at financial markets. The biologists use them for cell membrane recognition. The Federal Bureau of Investigation (FBI) considers wavelet application for storage of 30 million sets of criminal fingerprints [1]. The computer scientists exploit them in image processing like edge recognition, image searching, animation control, image compression and even Internet traffic description. The engineers use wavelet transforms for time phenomena study in transient processes. Recently, wavelets have been tested for structural health monitoring and damage detection. The ability to monitor a structure and detect damage at earliest possible stage becomes an important issue throughout the aerospace, mechanical and civil engineering communities.

The literature on wavelet transforms in the one-dimensional case is very extensive. Applicability of various wavelets in detection of cracks in beams has been studied by Douka et al. [2], Quek et al. [3] as well as Gentile and Messina [4]. Frame structures have been analysed by Ovanesova and Suarez [5]. For a practical application of the wavelet damage detection techniques research on experimental data is the most important. Hong et al. [6] and Douka et al. [2] showed that the effectiveness of wavelets for damage localization

*Corresponding author. Tel.: +48 58 347 24 97; fax: +48 58 347 16 70.
E-mail address: mrucka@pg.gda.pl (M. Rucka).

0022-460X/$ - see front matter © 2006 Elsevier Ltd. All rights reserved.
doi:10.1016/j.jsv.2006.04.015

is limited by the measurements precision and the sampling distances. They used the dynamic mode shapes extracted from the acceleration measurements. One accelerometer was kept as a reference input, while the second one was moved along the beam. They preformed the measurements in 39 points of the beam. For wavelet analysis the signal was oversampled to 390 points by a cubic spline interpolation. Rucka and Wilde [7] used the optic displacement measurement technique that allowed the high precision measurements of the beam static displacements in 81 points. Although current works show that only relatively large cracks can be detected, the search for the structural damage by wavelets is a promising and developing field of research.

The two-dimensional damage detection problems were addressed by Wang and Deng [8]. They analysed a steel plate with an elliptical hole and subjected to a uniform tensile loading. The static displacement field was determined by the analytical formula and was considered as input for the wavelet transform. The location of the crack tip was found by a variation of the Haar wavelet coefficients. Douka et al. [9] studied vibrations of a rectangular plate with a crack running parallel to one side of the plate. The one-dimensional wavelet transform was successfully applied to the analytically determined mode shapes along their vertical lines at different locations. Cracks of a relative depth varied from 10% up to 50% have been considered. The proposed intensity factor allowed estimation of the damage size. The works based on numerically computed plate mode shapes were presented by Chang and Chen [10] and Rucka and Wilde [11]. The wavelet transforms of the two-dimensional plate problems [8–11] were addressed by the one-dimensional wavelet analysis since the signal lines at the different locations have been treated separately. The two-dimensional discrete wavelet transform for detection of cracks in plates based on numerical data was presented by Loutridis et al. [12].

The experimental researches on plate damage detection have been presented by Wilde and Rucka [13]. The experimental mode shapes of the cantilever plate have been determined by the acceleration measurement in one point and impact excitation in 66 points. The relative depth of the introduced rectangular defect was about 19%. The location of the damage was determined by the Gaussian wavelet with four vanishing moments. However, the problem was approached by the one-dimensional wavelet formulation.

In this paper a method for estimating damage localization in a beam and plate is presented. The damage localization is based on the experimentally determined mode shapes of a cantilever beam and a plate with four fixed supports. For the plate problem the two-dimensional formulation of the wavelet transform is derived.

2. Continuous wavelet transform in damage detection

2.1. One-dimensional wavelet transform

A wavelet is an oscillatory, real or complex-valued function $\psi(x) \in \mathbf{L}^2(\mathbb{R})$ of zero average and finite length. Function $\psi(x)$ is called a mother wavelet and $\mathbf{L}^2(\mathbb{R})$ denotes the Hilbert space of measurable, square-integrable one-dimensional functions. In this paper, apart from general definition, only the real wavelets and the space domain will be considered. The function $\psi(x)$ localized in both space and frequency domains is used to create a family of wavelets $\psi_{u,s}(x)$ formulated as

$$\psi_{u,s}(x) = \frac{1}{\sqrt{s}}\psi\left(\frac{x-u}{s}\right), \tag{1}$$

where the real numbers s and u denote the scale and translation parameters, respectively.

For a given signal $f(x) \in \mathbf{L}^2(\mathbb{R})$, where x denotes spatial coordinate, the continuous wavelet transform (CWT) is the inner product of the signal function with the wavelet functions (e.g. Refs. [1,14,15]):

$$Wf(u,s) = \langle f, \psi_{u,s} \rangle = \frac{1}{\sqrt{s}} \int_{-\infty}^{+\infty} f(x)\psi\left(\frac{x-u}{s}\right) \mathrm{d}x, \tag{2}$$

where $Wf(u,s)$ is called a wavelet coefficient for the wavelet $\psi_{u,s}(x)$ and it measures the variation of the signal in the vicinity of u whose size is proportional to s. The integral form of the wavelet transform given by Eq. (2)

can be rewritten as a convolution product:

$$Wf(u,s)=\frac{1}{\sqrt{s}}\int_{-\infty}^{+\infty}f(x)\psi\left(\frac{-(u-x)}{s}\right)\mathrm{d}x=\frac{1}{\sqrt{s}}f*\psi\left(\frac{-u}{s}\right)=f*\overline{\psi}_s(u), \tag{3}$$

where $\overline{\psi}_s(x)=1/\sqrt{s}\psi(x/s)$.

Wavelets have scale and space aspects. Owing to this the space-scale view of signals, an important property of wavelets is their ability to react to subtle changes, breakdown points or discontinuities in a signal. In detection of singularities of signals the vanishing moments play an important role. A wavelet has n vanishing moments if the following equation is satisfied:

$$\int_{-\infty}^{+\infty}x^k\psi(x)\,\mathrm{d}x=0,\quad k=0,1,2,\ldots,n-1. \tag{4}$$

Hence the wavelet having n vanishing moments is orthogonal to polynomials up to degree n–1. Mallat [16] proved that for wavelets with n vanishing moments and a fast decay there exist function $\theta(x)$ with a fast decay defined as follows:

$$\psi(x)=\frac{\mathrm{d}^n\theta(x)}{\mathrm{d}x^n},\quad \int_{-\infty}^{+\infty}\theta(x)\,\mathrm{d}x\neq 0. \tag{5}$$

For $n=1$ a smoothing function $\theta(x)$ is the integral of a wavelet function $\psi(x)$ over $(-\infty,x)$ for each value of x:

$$\theta(x)=\int_{-\infty}^{x}\psi(u)\,\mathrm{d}u. \tag{6}$$

Therefore, a wavelet with n vanishing moments can be rewritten as the nth order derivative of a function $\theta(x)$. The resulting wavelet transform can be expressed as a multiscale differential operator:

$$\begin{aligned}Wf(u,s)&=\frac{s^n}{\sqrt{s}}\int_{-\infty}^{+\infty}f(x)\frac{\mathrm{d}^n}{\mathrm{d}x^n}\theta\left(\frac{x-u}{s}\right)\mathrm{d}x=\frac{s^n}{\sqrt{s}}\frac{\mathrm{d}^n}{\mathrm{d}x^n}\int_{-\infty}^{+\infty}f(x)\theta\left(\frac{-(u-x)}{s}\right)\mathrm{d}x\\&=\frac{s^n}{\sqrt{s}}\frac{\mathrm{d}^n}{\mathrm{d}u^n}f*\theta\left(\frac{-u}{s}\right)=s^n\frac{\mathrm{d}^n}{\mathrm{d}u^n}(f*\bar{\theta}_s)(u),\quad \bar{\theta}_s(x)=\frac{1}{\sqrt{s}}\theta\left(\frac{-x}{s}\right),\end{aligned} \tag{7}$$

where $f*\bar{\theta}_s$ denotes a convolution of functions. Thus wavelet transform is the nth derivative of the signal $f(x)$ smoothed by a function $\bar{\theta}_s(x)$ at the scale s. If the signal has a singularity at a certain point u, that means, it is not differentiable at u, then the CWT coefficients will have relatively large values. When the scale is large, the convolution with $\bar{\theta}_s(x)$ removes small signal fluctuation and therefore only detection of large variation is possible [16]. Singularities are detected by finding the abscissa where the maxima of the wavelet transform modulus $|Wf(u,s)|$ converge at fine scales [14]. If the wavelet has only one vanishing moment, wavelet modulus maxima are the maxima of the first-order derivative of $f(x)$ smoothed by $\bar{\theta}_s(x)$. If the wavelet has two of more vanishing moments, the modulus maxima correspond to higher derivatives.

The measured or calculated mode shape of a structure can be treated as a spatially distributed signal and the CWT can be computed for this signal. A sudden change or peak in the analysed wavelet coefficient can indicate the location of a crack. The possibility of damage detection by the Haar [3,8], Mexican Hat [6], Symlet [2,9,12], Coiflet [7], Gaussian [4,7,11,13,17] or biorthogonal wavelets [5] were discussed. The considered real wavelet characteristics are summarized in Table 1. The application of the complex-valued Gabor wavelet function has been considered in Refs. [3,8,10].

The selection of an appropriate type of a wavelet and the choice of its number of vanishing moments is essential for effective use of the wavelet analysis in damage detection. Hong et al. [6] proved that in the case of crack detection in beams the number of the vanishing moments should be at least 2. Douka et al. [2] stated that wavelets having higher number of vanishing moments provide more stable performance. However, since wavelets with higher number of vanishing moments have longer supports, the trade-off between the number of vanishing moments and the support sizes must be considered. Wavelets with two vanishing moments have shorter length but they produce wavelet coefficients different from zero on all length. Using wavelets that create maximum number of wavelet coefficients that are close to zero is proposed in this study. In the case of

Table 1
Real wavelet characteristics

Wavelet family name	Order N Order $N_r.N_d$	No. of vanishing moments	Symmetry	Support width	Existence of scaling function
Haar	—	1	Asymmetry	1	Yes
Daubechies N	$N = 1,2,\ldots$	N	Far from	$2N$–1	Yes
Symlet N	$N = 2,3,\ldots$	N	Near from	$2N$–1	Yes
Coiflet N	$N = 1,2,3,4,5$	$2N$	Near from	$6N$–1	Yes
Biorthogonal $N_r.N_d$	$N_r = 1$, $N_d = 1,3,5$	N_r –1	Yes ($N_r = 1,3$)	$2N_d+1$	Yes
	$N_r = 2$, $N_d = 2,4,6,8$				
	$N_r = 3$, $N_d = 1,3,5,7,9$				
	$N_r = 4$, $N_d = 4$		Asymmetry		
	$N_r = 5$, $N_d = 5$		($N_r = 2,4,5,6$)		
	$N_r = 6$, $N_d = 8$				
Reverse Biorthogonal $N_d.N_r$	$N_d = 1$, $N_r = 1,3,5$	N_d–1	Yes ($N_d = 1,3$)	$2N_r+1$	Yes
	$N_d = 2$, $N_r = 2,4,6,8$				
	$N_d = 3$, $N_r = 1,3,5,7,9$				
	$N_d = 4$, $N_r = 4$		Asymmetry		
	$N_d = 5$, $N_r = 5$		($N_d = 2,4,5,6$)		
	$N_d = 6$, $N_r = 8$				
Gaussian N	$N = 1,2,\ldots$	N	Yes (N even) Asymmetry (N odd)	10	No
Mexican hat	—	2	Yes	16	No

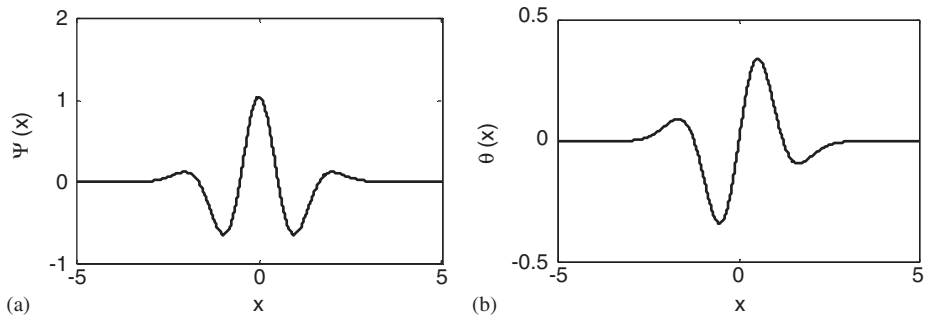

Fig. 1. Gaussian wavelet (gaus4): (a) wavelet function $\psi(x)$; (b) function $\theta(x)$.

structural mode shapes that are similar to a combination of polynomials of the fourth order, wavelet with four vanishing moments guarantee that non-zero values of the wavelet coefficients correspond only to the abnormalities of the signal. For structural responses that are similar to polynomial of higher order than 4, the use of wavelets with higher number of vanishing moments is necessary.

In this paper the Gaussian wavelet having four vanishing moments (gaus4) was chosen as the best candidate to damage detection with one-dimensional CWT of fundamental mode shape. The advantage of Gaussian wavelets has been discussed in Refs. [4,7,14]. The Gaussian wavelet function $\psi(x)$ with smoothing function $\theta(x)$ is shown in Fig. 1.

2.2. Two-dimensional wavelet transform

The one-dimensional wavelet transform can be extended to any dimensions [18]. In this section the two-dimensional case for plate structures damage localization is studied.

Let $f(x,y)$ be a signal belonging to the Hilbert $\mathbf{L}^2(\mathbb{R}^2)$ space of measurable, square-integrable two-dimensional functions. A horizontal wavelet $\psi^1(x,y)$ and a vertical one $\psi^2(x,y)$ (Fig. 3) are constructed with separable products of a scaling function ϕ and a wavelet function ψ (Fig. 2) [14]:

$$\psi^1(x,y) = \phi(x)\psi(y), \quad \psi^2(x,y) = \psi(x)\phi(y). \tag{8}$$

For two directions a family of wavelets can be written as

$$\psi^i_{u,v,s} = \frac{1}{s}\psi^i\left(\frac{x-u}{s}, \frac{y-v}{s}\right), \quad i = 1,2. \tag{9}$$

The wavelet transforms of the function $f(x,y)$ defined with respect to each of the wavelets given by Eq. (8) are formulated as follows:

$$\begin{aligned} W^i f(u,v,s) &= \left\langle f, \psi^i_{u,v,s} \right\rangle = \frac{1}{s}\int_{-\infty}^{\infty}\int_{-\infty}^{\infty} f(x,y)\psi^i\left(\frac{x-u}{s}, \frac{y-v}{s}\right) \mathrm{d}x\mathrm{d}y \\ &= \frac{1}{s} f * \psi^i\left(\frac{-u}{s}, \frac{-v}{s}\right) = f * \bar{\psi}^i_s(u,v), \quad i = 1,2. \end{aligned} \tag{10}$$

Two wavelets $\psi^1(x,y)$ and $\psi^2(x,y)$ can be defined as the partial derivatives of the smoothing function $\theta(x,y)$ along x and y coordinates:

$$\psi^1(x,y) = \frac{\partial^n \theta(x,y)}{\partial x^n}, \quad \psi^2(x,y) = \frac{\partial^n \theta(x,y)}{\partial y^n}, \tag{11}$$

where indices 1 and 2 denote a horizontal and vertical direction, respectively, and n is a number of vanishing moments. Two scaled wavelets can be rewritten in the form:

$$\psi^1_s(x,y) = \frac{\partial^n \theta_s(x,y)}{\partial x} = s^n \frac{\partial \theta(x,y)}{\partial x}, \quad \psi^2_s = \frac{\partial^n \theta_s(x,y)}{\partial y} = s^n \frac{\partial \theta(x,y)}{\partial y} \tag{12}$$

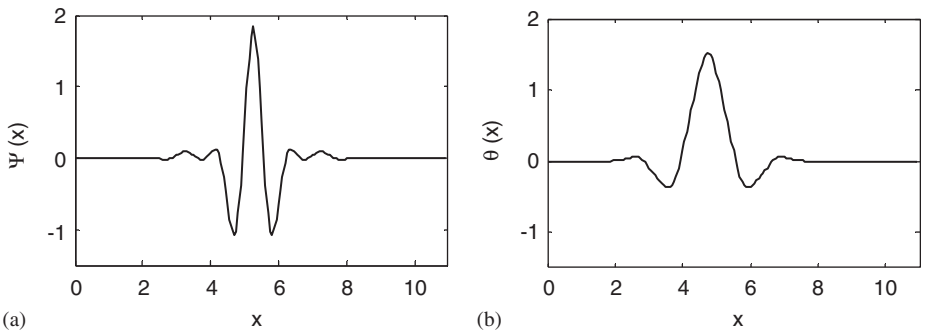

Fig. 2. Reverse biorthogonal wavelet (rbio5.5): (a) wavelet function $\psi(x)$; (b) scaling $\phi(x)$ function.

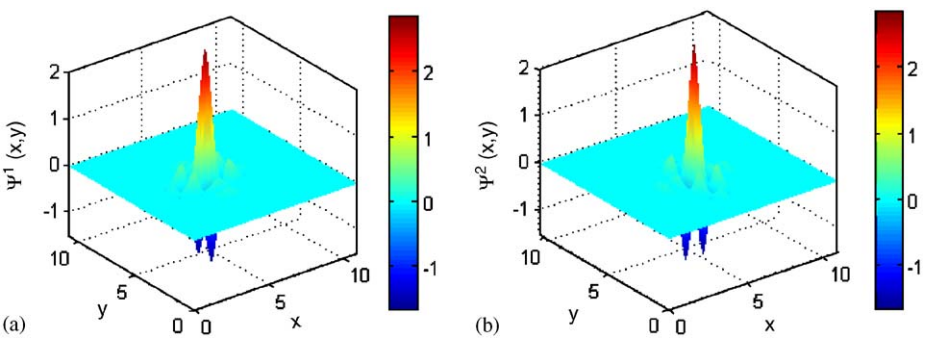

Fig. 3. Horizontal wavelet $\psi^1(x,y)$ and vertical wavelet $\psi^2(x,y)$ functions of rbio5.5.

A scaled smoothing function $\theta(x,y)$ is given by

$$\theta_{u,v,s}(x,y)=\frac{1}{s}\theta\left(\frac{x-u}{s},\frac{y-v}{s}\right). \tag{13}$$

Finally, a derivative form of the wavelet transform can be expressed as

$$\begin{pmatrix} W^1f(u,v,s)\\ W^2f(u,v,s)\end{pmatrix}=\begin{pmatrix} f*\bar{\psi}_s^1(u,v)\\ f*\bar{\psi}_s^2(u,v)\end{pmatrix}=\begin{pmatrix} f*s^n\frac{\partial\bar{\theta}_s}{\partial u}(u,v)\\ f*s^n\frac{\partial\bar{\theta}_s}{\partial v}(u,v)\end{pmatrix}=s^n\begin{pmatrix}\frac{\partial}{\partial u}(f*\bar{\theta}_s)(u,v)\\ \frac{\partial}{\partial v}(f*\bar{\theta}_s)(u,v)\end{pmatrix}$$
$$=s^n\overrightarrow{\nabla}(f*\bar{\theta}_s)(u,v), \tag{14}$$

where $\bar{\theta}_{u,v,s}=\theta_{u,v,s}(-x,-y)$. Therefore, the wavelet transform components of the derivative form given by Eq. (13) can be interpreted as the coordinates of gradient vector of $f(x,y)$ smoothed by $\bar{\theta}_s(x,y)$. The $W^1f(u,v,s)$ wavelet component indicates horizontal edges while the $W^2f(u,v,s)$ component indicates vertical edges. The names of these components are derived from image processing.

The function

$$Mf(u,v,s)=\sqrt{\left|W^1f(u,v,s)\right|^2+\left|W^2f(u,v,s)\right|^2} \tag{15}$$

is called the modulus of the wavelet transform at the scale s. Function (15) is proportional to the modulus of the gradient vector $\vec{\nabla}(f*\bar{\theta}_s)(x,y)$. The modulus $Mf(u,v,s)$ has local maxima in the direction of the gradient given by

$$Af(u,v,s)=\arctan\left(\frac{W^2f(u,v,s)}{W^1f(u,v,s)}\right). \tag{16}$$

The angle between the gradient vector $\vec{\nabla}(f*\bar{\theta}_s)(x,y)$ and the horizontal direction indicate locally the direction, where the signal has the sharpest variation [19]. The direction of the gradient vector at point (x_0,y_0) indicates the direction in the plane (x,y) along which the directional derivative of $f(x,y)$ has the largest absolute value.

In this paper the reverse biorthogonal wavelet with four vanishing moments (rbio5.5) is applied. This wavelet provided the best effectiveness in detecting crack position. The selection has been based on simulations with all wavelets given in Table 1 and experimental data presented in the following sections. The performance of the reverse biorthogonal wavelet is similar to Gaussian and it has a scaling function. The reverse biorthogonal wavelet function $\psi(x)$ and its scaling function $\phi(x)$ are plotted in Fig. 2.

3. Experimental investigations to determine plate mode shapes

3.1. Experimental set-up

A cantilever beam and a plate with four fixed supports are considered. The beam (Fig. 4) of length $L=480\,\text{mm}$, width $B=60\,\text{mm}$ and height $H=20\,\text{mm}$ is made of polymethyl methacrylate (PMMA), sold

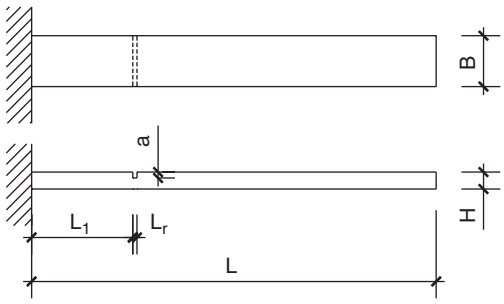

Fig. 4. Geometry of the cracked beam.

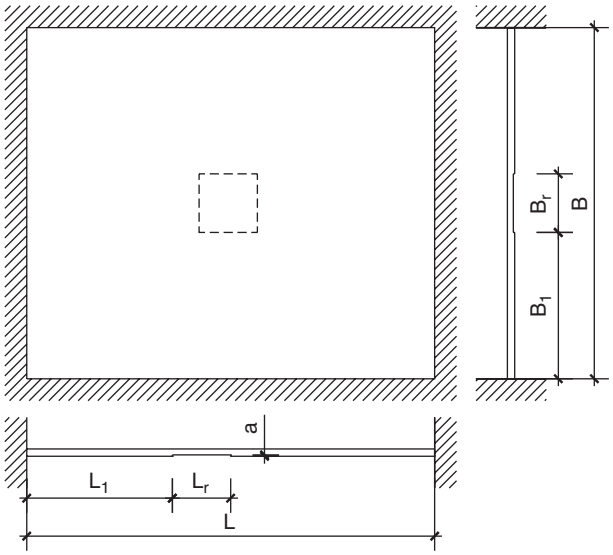

Fig. 5. Geometry of the plate with defect.

by the tradenames Plexiglas. The experimentally determined material properties are: Young's modulus $E = 3420\,\text{MPa}$, Poisson ratio $v = 0.32$ and mass density $\rho = 1187\,\text{kg/m}^3$. The beam contains an open crack of length $L_r = 2\,\text{mm}$ and height $a = 7\,\text{mm}$ at a distance $L_1 = 120\,\text{mm}$ from the clamped end. The depth of the crack is 35% of beam height.

The steel plate of length $L = 560\,\text{mm}$, width $B = 480\,\text{mm}$ and height $H = 2\,\text{mm}$ is shown in Fig. 5. Experimentally determined material properties are: Young's modulus $E = 192\,\text{GPa}$, Poisson ratio $v = 0.25$ and mass density $\rho = 7430\,\text{kg/m}^3$. The plate contains a rectangular defect of length $L_r = 80\,\text{mm}$, width $B_r = 80\,\text{mm}$ and height of $a = 0.5\,\text{mm}$. The distance from the defect left–down corner to the plate left–down corner in horizontal and vertical directions are $L_1 = 200\,\text{mm}$ and $B_1 = 200\,\text{mm}$, respectively. The area of the flaw amounts to 2.4% of the plate area and the depth of the flaw is 25% of the plate height.

The beam was subjected to a dynamic pulse load applied at 48 points along the length of the beam perpendicular to the beam axis whereas the plate was subjected to the pulse load applied at 143 points situated on its surface. Black dotes, plotted in Fig. 6 indicate the points of load application. The measurements were made using one accelerometer to record the response of the structure. Dynamic pulse load was induced by the modal hammer PCB 086C03. The data were collected by the data acquisition system Pulse type 3650C.

3.2. Mode shape estimation

Any discrete system can be described by equation of motion:

$$\mathbf{M}\ddot{\mathbf{x}}(t) + \mathbf{C}\dot{\mathbf{x}}(t) + \mathbf{K}\mathbf{x}(t) = \mathbf{F}(t), \tag{17}$$

where $\mathbf{M}$, $\mathbf{C}$, $\mathbf{K}$ are the mass, damping and stiffness matrices, respectively. Laplace transform of equation of motion (17) gives:

$$(\mathbf{M}s^2 + \mathbf{C}s + \mathbf{K})\mathbf{X}(s) = \mathbf{F}(s), \tag{18}$$

where s is a Laplace variable. Eq. (18) can be rewritten as

$$\mathbf{B}(s)\mathbf{X}(s) = \mathbf{F}(s), \tag{19}$$

where $\mathbf{B}(s)$ known as a system matrix. Transfer function matrix is defined as follows (e.g. Ref. [20]):

$$\mathbf{H}(s) = \mathbf{B}(s)^{-1} \tag{20}$$

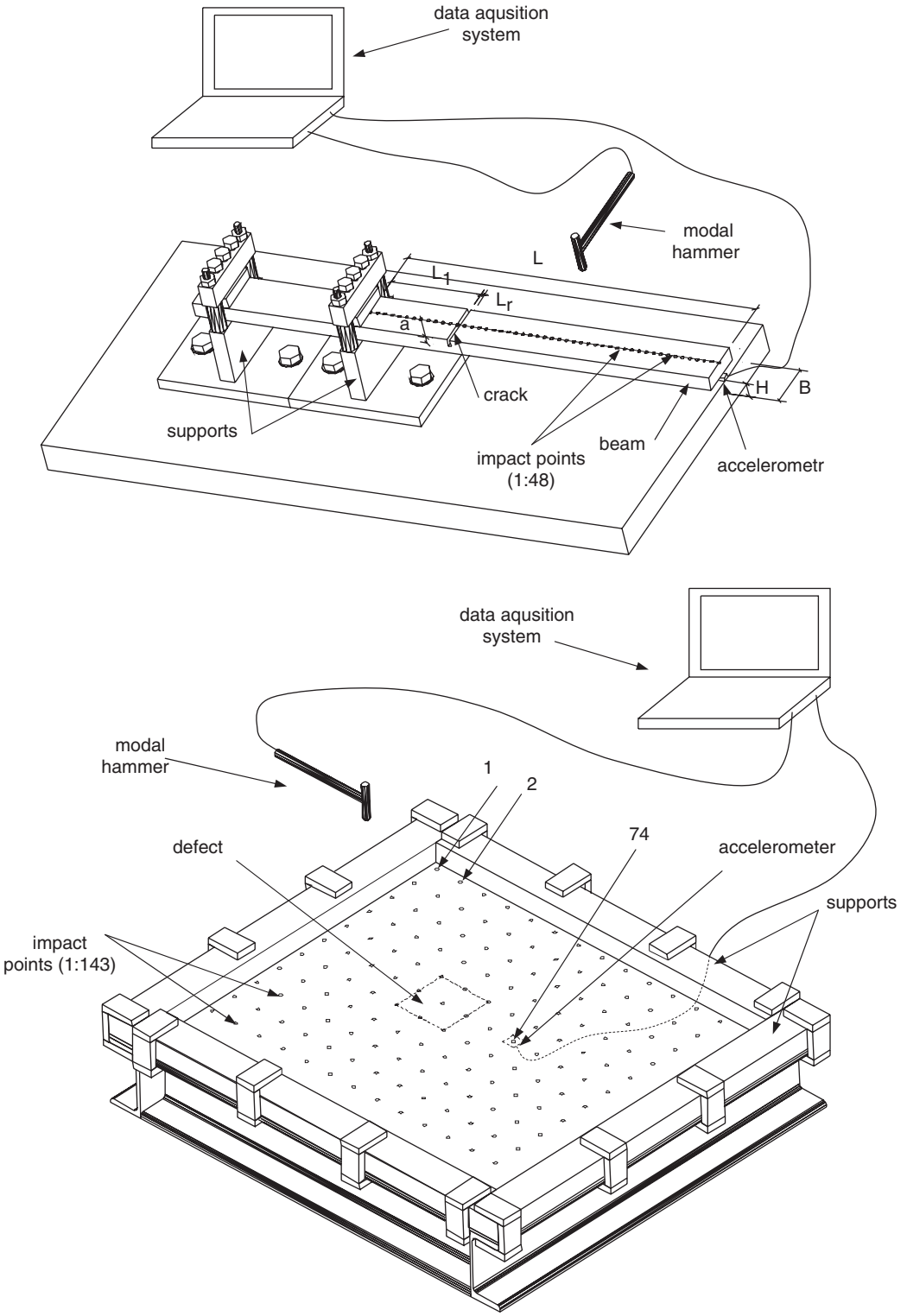

Fig. 6. Experimental set-up.

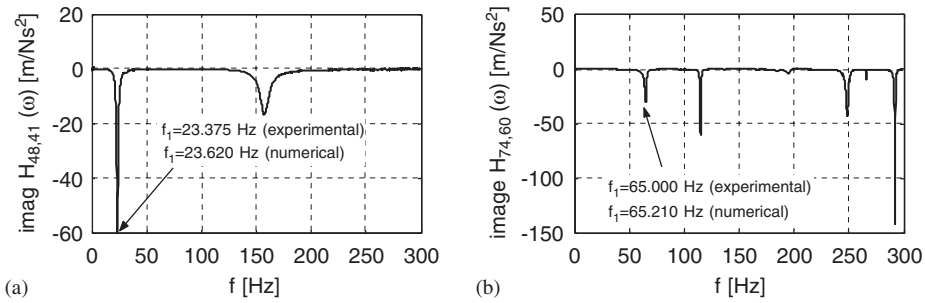

Fig. 7. Frequency response function for the: (a) beam; (b) plate.

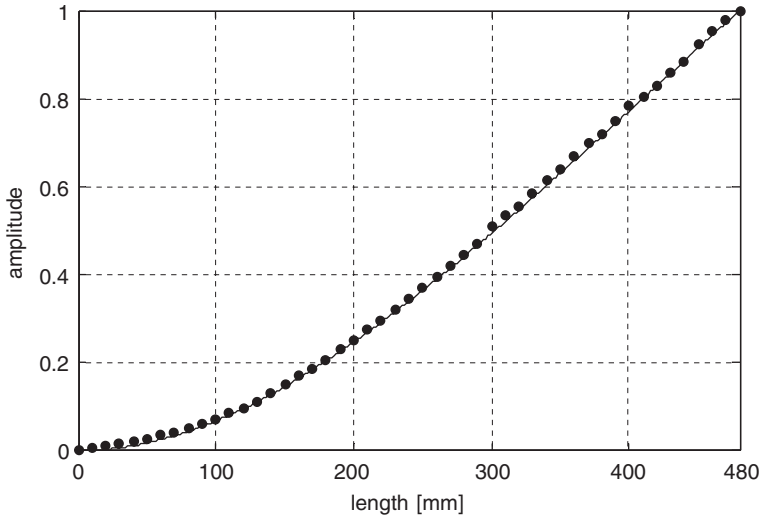

Fig. 8. Fundamental mode shape for the beam; — numerical mode shape, ● experimental mode shape.

Evaluating the transfer function matrix along the frequency axis ($s = \mathrm{i}\omega$) results in frequency response function (FRF) matrix given as

$$\mathbf{H}(\omega) = \mathbf{X}(\omega)[\mathbf{F}(\omega)]^{-1}. \tag{21}$$

Matrix $\mathbf{H}$ of size $m \times m$, where m denotes a number of degrees of freedom, contains individual FRFs $H_{jk}(\omega)$ obtained by impacting point k and measuring the response at point j. To determine one row of the FRF matrix $\mathbf{H}(\omega)$ the modal hammer signal is measured in all points whereas the acceleration is measured still in the same one point. Mode shape is contained in each row or columns of FRF matrix. The most informative is the imaginary part of FRF since it shows both the amplitude and the direction of the response. An example of the beam FRF is shown in Fig. 7a. The function $H_{48,41}(\omega)$ is obtained by impacting the beam at point 41 and measuring the response at point 48. The example of the FRF $H_{74,60}(\omega)$ for the plate is presented in Fig. 7b. The obtained FRFs allowed precise identification of the structures lowest frequencies. The experimental first frequency of the beam was found to be $f_1 = 23.375\,\mathrm{Hz}$. The fundamental frequency of the plate was $f_1 = 65.0\,\mathrm{Hz}$. The experimentally determined mode shapes for the beam and plate are given in Figs. 8 and 9b, respectively.

4. Numerical mode shapes of beam and plate

The mode shapes for the notched beam and plate were computed by the commercial FEM program SOFiSTiK. The beam mode shape was calculated using a solid six-sided element of length 2 mm. The mode shapes of the plate were computed using square plane element of the size $40 \times 40\,\mathrm{mm}$. The first calculated

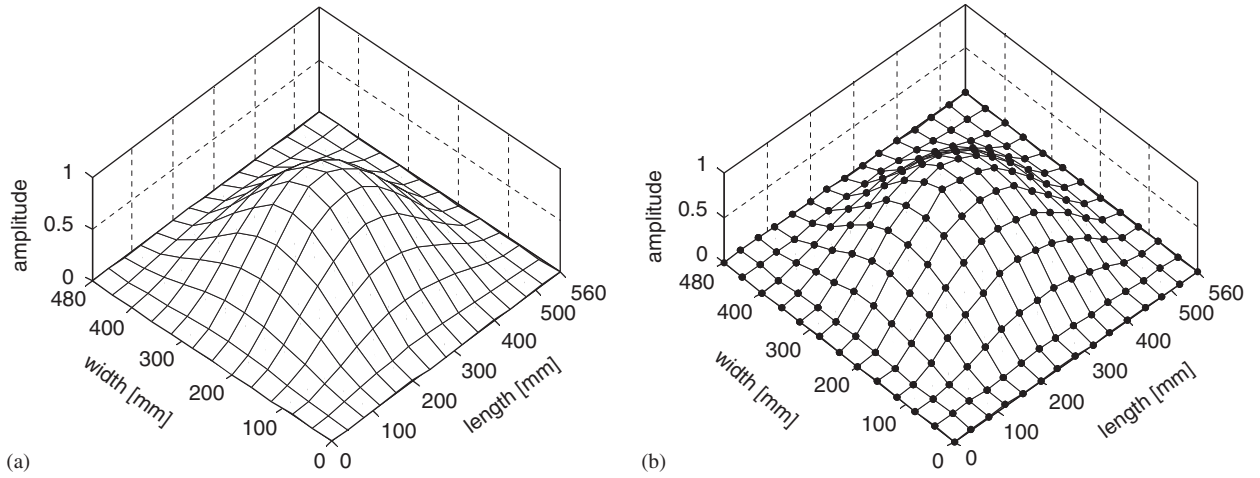

Fig. 9. Fundamental mode shape for the plate: (a) numerical; (b) experimental.

frequency for the beam is $f_1 = 23.62\,\text{Hz}$ while the plate first frequency is $f_1 = 65.21\,\text{Hz}$. The computed frequencies of both structures are very similar to the experimentally obtained frequencies. A comparison between the numerical and experimental mode shapes is given in Figs. 8 and 9. The beam experimental mode shape (Fig. 7) is slightly underestimated for the region near the support. This discrepancy is due to the difficulties in obtaining an ideal fixed support of the beam. The first numerical and experimental mode shapes of the plate (Figs. 9a and b) have to be presented separately since the obtained results are almost identical.

Since the mode shape of the beam was measured with sampling distance of 10 mm and calculated with sampling distance of 2 mm, a piecewise cubic spline data interpolation is used to decrease sampling distance to 1 mm. The mode shape of the plate is also interpolated to decrease sampling distance from 40 to 1 mm. Then each mode shape line is normalized to 1.

5. Results of the wavelet analysis

5.1. Border distortion problem

The CWT is defined as integration of the product of a wavelet and a signal of infinite length. Since mode shape of the beam $f(x)$ as well as the mode shape of the plate $f(x, y)$ are signals of finite length a border distortion problem appears. The wavelet coefficients achieve an extremely high value at the ends of a signal and those values do not indicate damage. Therefore, the border of the signal should be treated independently from the rest of the signal. The influence of boundary effects can be reduced by extension from the signal beyond the boundary. It is obvious that the length of the extended signal depends on the scale of the used wavelet. The edge effect width can be estimated as a half-width of the wavelet with the highest scale. In this paper, to avoid large discrepancy at the boundaries, the signal is extended outside its original support by a cubic spline extrapolation [1,15] based on four neighbouring points. The spline provides a technique for obtaining a smoother extrapolation. The extrapolation is continuous, with continuous first and second derivative. However, the fourth derivative, used in this paper, is allowed to have jumps at the connection points. Therefore, the integration of the wavelet function with the mode shape near the location of the plate edges can result in small non-zero values of the CWT coefficients.

5.2. One-dimensional wavelet transform of beam mode shape

The wavelet analysis is conducted on beam fundamental mode shape assumed as a spatially distributed signal by the Gaussian wavelet family. The wavelet analysis is performed using gaus4 wavelet having four vanishing moments, because the first beam mode shape is similar to polynomial of fourth order. The wavelet

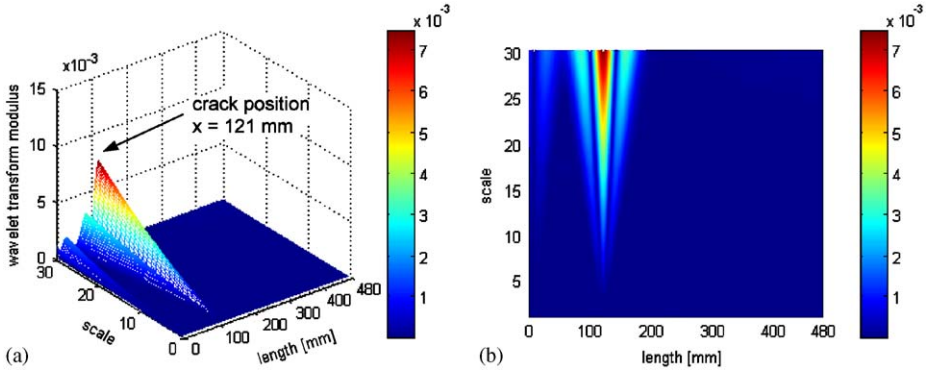

Fig. 10. Wavelet transform modulus of numerical first mode shape; (a) 3D view; (b) top view.

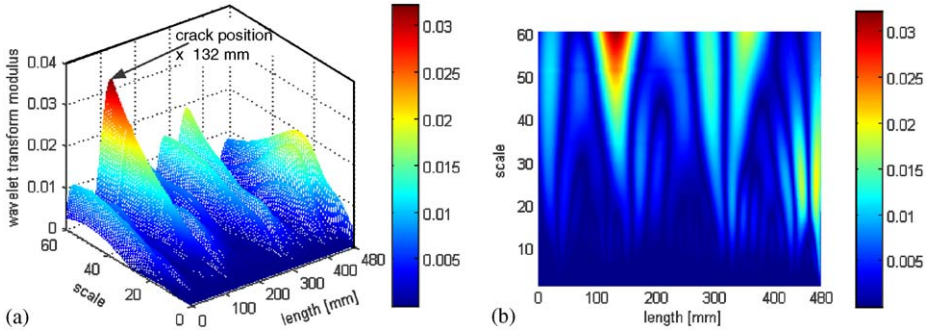

Fig. 11. Wavelet transform modulus of experimental first mode shape; (a) 3D view; (b) top view.

transform modulus computed from the first numerical mode shape is shown in Fig. 10. The one-dimensional CWT of numerical mode shapes is performed for scales $s = 1$–30. The modulus maximum value grows with the increase of the scale and clearly points to the crack position at 121 mm from the clamped end. The wavelet transform modulus results based on the experimental data (Fig. 11) have additional maxima lines resulting from the measurement noise. Nevertheless, the dominant maxima lines, corresponding to the crack positions, increases monotonically and for larger scales they achieve the largest values. The crack location can be easy recognized. Position of defect determined by wavelet analysis is 132 mm. The relative error between the identified crack centre and the its real position reaches 9.1%. The wavelet transforms of experimental mode shapes require larger values of scales than wavelet transforms of numerical mode shapes. In the case of experimental data crack positions cannot be detected for scales up to about 40 whereas in the case of numerical data crack positions can be determined from scale 2.

5.3. *Two-dimensional wavelet transform of plate mode shape*

In the case of two-dimensional signals, the space-scale representation of a signal is a three-dimensional problem (x,y,s). In order to limit the computation as well as the memory requirements it is possible to change continuous scale to scale variations limited to dyadic sequence ($s = 2^j$) leading to discrete wavelet transform (DWT). This approach can be successfully used in the case of the image processing for edge detection, where the analysis is conducted at fine scales. However, in the case of damage location in structures, higher scales are necessary. Between scale $s = 32$ and 64 there is a big gap in wavelet resolution and important piece of information might be lost. Therefore, costs of computations cannot be limited in this case and application of continuous scales is recommended.

The results of the wavelet transform of the plate fundamental mode shape are wavelet coefficients for different scales. A presence of the defect is detected by a sudden change in a spatial variation of the transformed response. The horizontal coefficients $W^1f(u,v,s)$, the vertical coefficients $W^2f(u,v,s)$ and the wavelet transform moduli $Mf(u,v,s)$ for the numerical and experimental data are given in Figs. 12 and 13, respectively. The results presented in Figs. 12 and 13 are computed at scale $s=40$. In the case of damage detection application, the $W^1f(u,v,s)$ wavelet component indicates the signal abnormalities along the width of the plate, i.e., along the y coordinate. This is because the detecting action is performed by function ψ along y coordinate. The $W^2f(u,v,s)$ component indicates the abnormalities along the length of the plate. Although the coefficient $W^1f(u,v,s)$ presented in the first row of the Fig. 12 is computed for the two-dimensional approach, the coefficient lines along the y coordinate resemble the shape of the wavelet function $\psi(y)$. By analogy, the lines of the vertical coefficient along x coordinate resemble the $\psi(x)$ function. The distribution of the horizontal and vertical coefficients in x and y directions is similar, which suggests that the shape of the defect

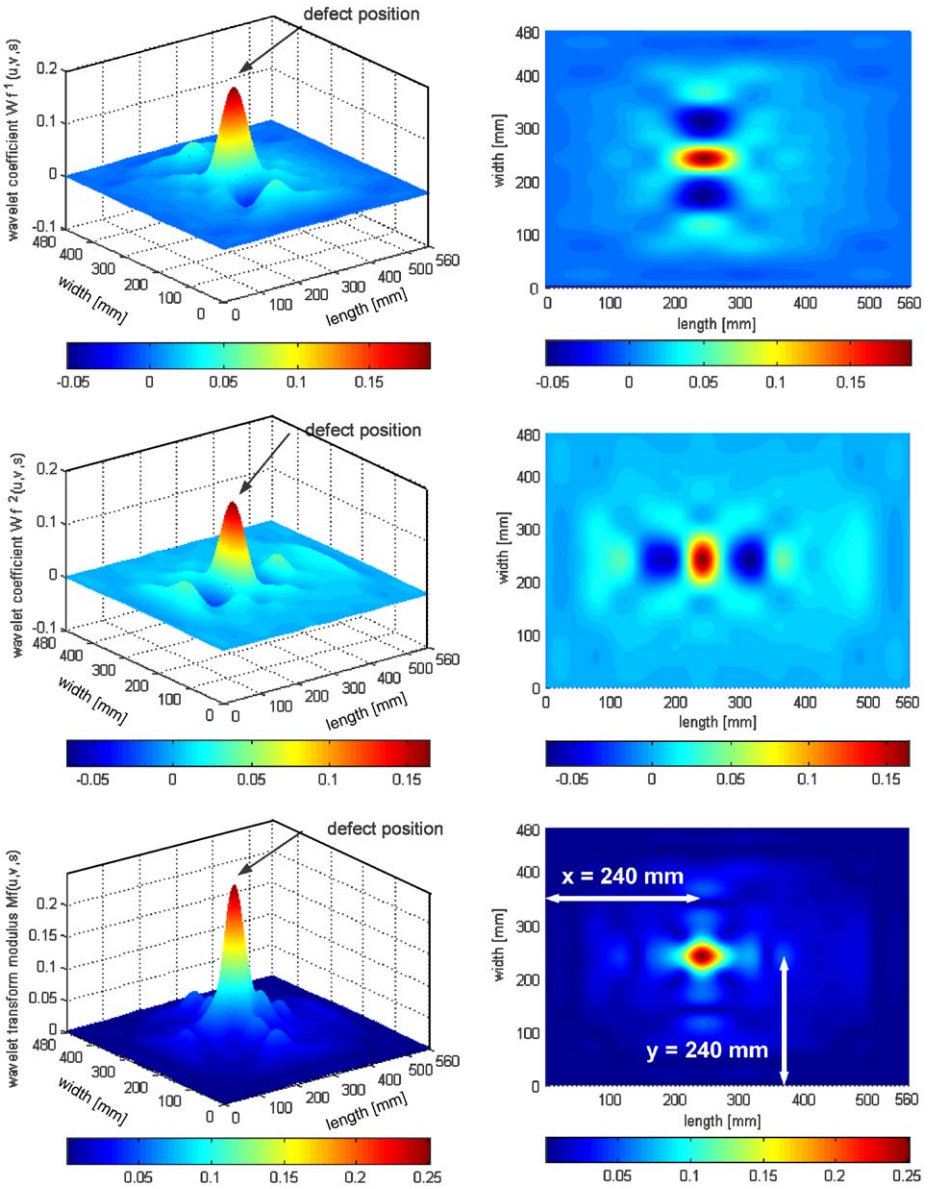

Fig. 12. Wavelet coefficients and wavelet transform modulus for the plate using rbio5.5 wavelet based on numerical data.

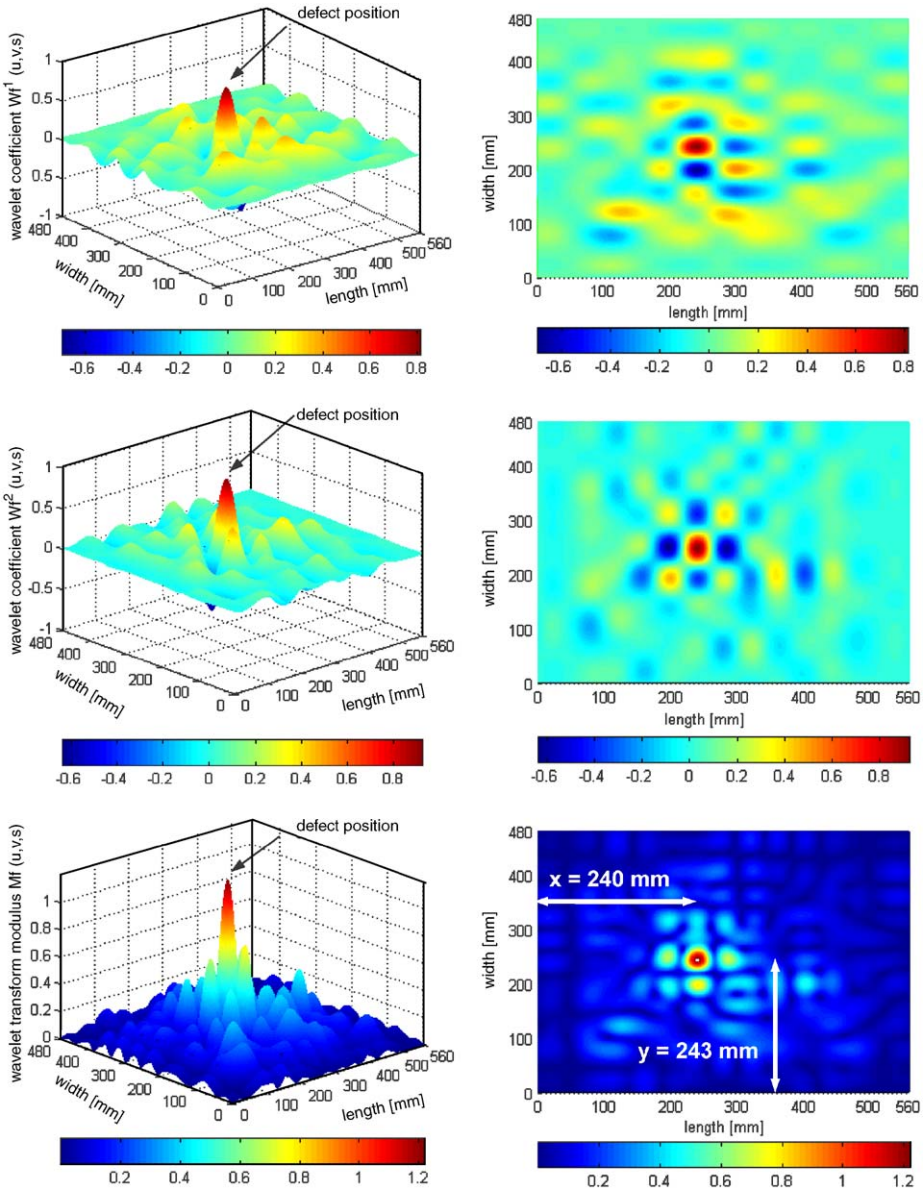

Fig. 13. Wavelet coefficients and wavelet transform modulus for the plate using rbio5.5 wavelet based on experimental data.

has similar dimensions in both directions. The third row of the Fig. 12 presents the modulus of the 2D wavelet coefficients and the visible cross, on the top view plot, combines the information stored in the $W^1f(u,v,s)$ and $W^2f(u,v,s)$ wavelet transform components.

The peak in the modulus $Mf(u,v,s)$ based on numerical (Fig. 12) as well as $Mf(u,v,s)$ based on the experimental data (Fig. 13) clearly indicates the defect position and its shape. In the case of the experimental data, the presence of some noise does not mask the signal abnormalities and the position and the size of the crack can be estimated. The local maximum of $Mf(u,v,s)$ based on the experimental data is in the distance of $x = 240$ mm and $y = 243$ mm from the left–down plate corner. The real location of defect is $x = 240$ mm and $y = 240$ mm from the left–down plate corner and it is in agreement with the maximum from numerical data. Difference between the recognized by wavelets defect centre position with actual one amount 1.25% in the vertical direction and there is no difference in the horizontal direction. The maximum value of the

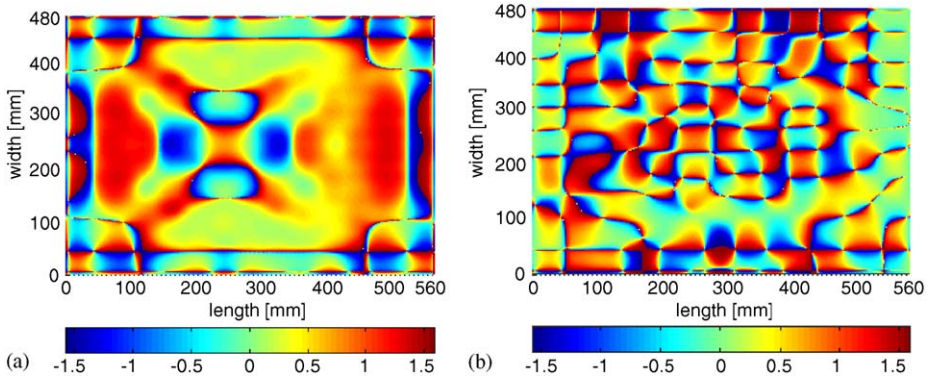

Fig. 14. Angle of the wavelet transform vector: (a) numerical data; (b) experimental data.

experimental wavelet transform modulus $Mf(u,v,s)$ is about four times larger than the corresponding numerical modulus.

Additional information about the defects can be obtained from analysis of the angle $Af(u,v,s)$ However, in the case of the experimental data the noise corrupts the information contained in the angle plot. Since the coefficients $W^1f(u,v,s)$ and $W^2f(u,v,s)$ often change signs, therefore the angle of the gradient vector $\vec{\nabla}(f * \bar{\theta}_s)(x,y)$ quickly changes its values (Fig. 14b). Therefore, it is impossible to directly locate the defect position from experimental data. The angle plot obtained from the numerical data (Fig. 14a) points the defect position by indicating the direction with sharpest signal variations.

6. Conclusions

The presented work is devoted to the wavelet-based damage detection techniques in beam and plate structures. The wavelet transforms are applied to fundamental mode shapes of the beam and plate. The mode shapes are determined experimentally and numerically. The one-dimensional wavelet analysis has been extended for application in two-dimensional structures. The formulation of the wavelet transform for two-dimensional plate problems is presented.

The study on wavelet analysis applied in damage detection leads to the following conclusions and suggestions:

1. CWT are more suitable for damage detection than DWT. The CWTs provide precise resolution necessary for damage localization.
2. The border distortion problem must be addressed. At least the first and second derivative of the extrapolation, outside the geometric boundary conditions, must be continuous.
3. Symmetric wavelets are appropriate for beam and plate damage detection. The considered Gaussian and reverse biorthogonal wavelets proved to be effective in the presented examples.
4. The wavelet transforms act as differential operators providing the information on signal derivatives. The order of the derivative is equal to the number of the vanishing moments.
5. The number of vanishing moments of the applied wavelet must be at least two. However, it has been shown that better resolution of the transformed response is obtained with wavelets having four and more vanishing moments.
6. The two-dimensional wavelet transform has been adopted and applied for two-dimensional structure responses. Modulus and gradient of two-dimensional wavelet transform are good indices of the damage localization.
7. Dynamic impulse tests and estimation of FRF provides easy and precise method for mode shape identification for the considered beam and plate.
8. The wavelet detection method might localize even small flaws in plate structures. The development of the damage detection techniques based on wavelet analysis is on a very early stage. Further studies towards

high quality measurements and application of statistical pattern recognition techniques should be conducted.

References

[1] G. Strang, T. Nguyen, *Wavelets and Filter Banks*, Wellesley-Cambridge Press, 1996.
[2] E. Douka, S. Loutridis, A. Trochidis, Crack identification in beams using wavelet analysis, *International Journal of Solid and Structures* 40 (2003) 3557–3569.
[3] S.T. Quek, Q. Wang, L. Zhang, K.K. Ang, Sensitivity analysis of crack detection in beams by wavelet technique, *International Journal of Mechanical Science* 43 (2001) 2899–2910.
[4] A. Gentile, A. Messina, On the continuous wavelet transforms applied to discrete vibrational data for detecting open cracks in damaged beams, *International Journal of Solid and Structures* 40 (2003) 295–315.
[5] A.V. Ovanesova, L.E. Suarez, Application of wavelet transform to damage detection in frame structures, *Engineering Structures* 26 (2004) 39–49.
[6] J.C. Hong, Y.Y. Kim, H.C. Lee, Y.W. Lee, Damage detection using Lipschitz exponent estimated by the wavelet transform: applications to vibration modes of beam, *International Journal of Solid and Structures* 39 (2002) 1803–1846.
[7] M. Rucka, K. Wilde, Crack identification using wavelets on experimental static deflection profiles, *Engineering Structures* 28 (2006) 279–288.
[8] Q. Wang, X. Deng, Damage detection with spatial wavelets, *International Journal of Solid and Structures* 36 (1996) 3443–3468.
[9] E. Douka, S. Loutridis, A. Trochidis, Crack identification in plates using wavelet analysis, *Journal of Sound and Vibration* 270 (2004) 279–295.
[10] C.C. Chang, L.W. Chen, Damage detection of a rectangular plate by spatial wavelet based approach, *Applied Acoustic* 65 (2004) 819–832.
[11] M. Rucka, K. Wilde, Numerical simulation of damage detection in rectangular plate by two-dimensional wavelet transform, *Proceedings of International Workshop on Simulations in Urban Engineering*, Gdansk, Poland, 2004, pp. 205–208.
[12] S. Loutridis, E. Douka, L.J. Hadjileontiadis, A. Trochidis, A two-dimensional wavelet transform for detection of cracks in plate, *Engineering Structures* 27 (2005) 1327–1338.
[13] K. Wilde, M. Rucka, Damage detection in rectangular plates by continuous two-dimensional wavelet transform, *Eurodyn 2005 Conference*, Paris, France, 1935–1940.
[14] S. Mallat, *A Wavelet Tour of Signal Processing*, Academic Press, New York, 1998.
[15] M. Misiti, Y. Misiti, G. Oppenheim, J. Poggi, *Wavelet Toolbox*, The MathWorks Inc, 2000.
[16] S. Mallat, S. Zhong, Characterization of signals from multiscale edges, *IEEE Transaction on Pattern Analysis and Machine Intelligence* 14 (1992) 710–732.
[17] A. Messina, Detecting damage in beams through digital differentiator filters and continuous wavelet transforms, *Journal of Sound and Vibration* 272 (2004) 385–412.
[18] S. Mallat, A theory for multiresolution signal decomposition: the wavelet representation, *IEEE Transaction on Pattern Analysis and Machine Intelligence* 11 (1989) 674–693.
[19] S. Mallat, W.L. Hwang, Singularity detection and processing with wavelet, *IEEE Transaction on Information Theory* 38 (1992) 617–643.
[20] N.M.M. Maia, J.M.M. Silva, *Theoretical and Experimental Modal Analysis*, Research Studies Press Ltd., England, 1997.